Electrodeposition of FeW-graphene composites: Effect of graphene oxide concentration on microstructure, hardness and corrosion properties

FlatChem 40 (2023) 100525

Contents lists available at ScienceDirect

FlatChem

journal homepage: www.sciencedirect.com/journal/flatchem

Electrodeposition of FeW-graphene composites: Effect of graphene oxide concentration on microstructure, hardness and corrosion properties

Antonio Mulone [a,*], Zhenyuan Xia [a,b], Uta Klement [a]

[a] Chalmers University of Technology, Department of Industrial and Materials Science, Gothenburg, Sweden
[b] Consiglio Nazionale delle Ricerche, Istituto per la Sintesi Organica e la Fotoreattività, Bologna, Italy

ARTICLE INFO

Keywords:
Electrodeposition
Graphene
Raman
Hardness
Corrosion

ABSTRACT

Graphene has emerged as excellent reinforcement for electrodeposited metallic composites. The poor stability of graphene in electrochemical baths makes it challenging to obtain uniform composite coatings. In this work, we investigate the possibility to electrodeposit FeW-graphene coatings with organic stablizers. Polydiallyldimethylammonium chloride is selected to stabilize the graphene oxide which is added into the electrolyte in various concentrations. Scanning electron microscopy and Raman analysis confirmed the successful co-deposition of graphene in all the coatings. The composition of the FeW matrix remained unaffected by the addition of graphene, while an increase in the crystallinity of the structure of the composites was observed. Graphene was retained even after the coatings were heat treated at 400 °C for 1 h. The hardness and the corrosion resistance of the FeW-graphene composite were largely improved: a 22% increase in hardness and an 80% increase in corrosion resistance were measured compared to the graphene-free coating.

1. Introduction

Recently electrodeposited Fe-based coatings have gained scientific interest as a potential sustainable alternative to chrome plating [1,2]. Thanks to the excellent properties obtained with chrome plating, hard chromium coatings have been largely applied in various fields ranging from aerospace [3] to automotive [4] applications. Despite their outstanding properties, the production of chrome coatings requires the use of cancerogenic compounds, i.e. hexavalent chromium [5]. Therefore, the search for new sustainable alternatives to chrome coatings is still a matter of great scientific interest.

Among the different electrodeposited Fe-based alloys, Fe-W alloys have gained significant attention for their advantages: (i) they can be deposited from thermodynamically stable and environmentally friendly electrolytes [6], (ii) composition and structure of the coatings can be tuned to optimize the properties for targeted applications [7], (iii) W-rich coatings exhibit hardness and thermal stability that exceed those of Co– or Ni-based alloys [8]. Furthermore, the hardness can be substantially increased with heat treatments [9,10], whereas the co-deposition of alumina particles has shown to dramatically improve the wear resistance [11]. The combination of co-deposition of alumina particles and optimal heat treatments can therefore result in mechanical properties and wear resistance that surpass those of hard chrome coatings [2]. Despite the impressive achievements obtained, few challenges remain to be solved. In fact, the corrosion resistance of the FeW alloys is quite low and it is hardly changed by the co-deposition of Al_2O_3 particles [11]. Furthermore, in order to improve both hardness and wear resistance of the FeW-Al_2O_3 composites, heat-treatments are recommended [2]. Therefore, the possibility to obtain an Fe-based coating with improved corrosion resistance and optimal hardness and wear resistance in the as-deposited condition remains a topic of great interest.

Since its scientific discovery, graphene and related graphenaceous materials, e.g. graphene nanoplatelets (GNPs), graphene oxide (GO) etc., have gained tremendous interest thanks to their superior corrosion [12] and mechanical resistance [13], and electrical and thermal properties [14,15]. In addition to the mentioned properties, layered-graphene can act as an excellent solid lubricant thanks to its stacked-planar structure [16]. The electrodeposition of various metals and alloys with graphenaceous compounds has already been performed successfully as reported in literature. For example, Pavithra et al. have shown that the co-deposition of graphene in Cu coatings resulted in an increase of the mechanical properties (i.e. 96% in hardness and 30% increase in elastic modulus), as compared to pure Cu foils [17]. Singh et al. reported that electrodeposited Ni-graphene coatings were

* Corresponding author.
E-mail address: mulone@chalmers.se (A. Mulone).

https://doi.org/10.1016/j.flatc.2023.100525
Received 1 March 2023; Received in revised form 29 June 2023; Accepted 2 July 2023
Available online 3 July 2023

Table 1
Constituents of the electrolyte and electrodeposition operating parameters.

Constituents	Parameter
Citric acid	0.3 M
Glycolic acid	1 M
$Fe_2(SO_4)_3$	0.1 M
Na_2WO_4	0.3 M
Surfactant	1, 2.5 and 5 g/L
GO	0.1, 0.5 and 1 g/L
pH	6.5
Temperature	65 ℃
Current density	40 mA/cm^2
Electrolyte agitations	250 rpm
Deposition time	1, 2 h

Table 2
Average particle size of GO in FeW-PDDA electrolytes.

Sample	Particle average size/PSD
GO	1192 ± 55 nm
FeW – 1 g/L PDDA– 0.1 g/L GO	4832 ± 45 nm
FeW – 5 g/L PDDA- 0.1 g/L GO	2374 ± 182 nm
FeW – 5 g/L PDDA – 0.5 g/L GO	1867 ± 77
FeW – 5 g/L PDDA – 1 g/L GO	8315 ± 195

characterized with ten times higher wear resistance as compared to pure Ni [18], whereas the addition of graphene resulted in an increase of the corrosion resistance in Zn-Ni [19] and in Fe-based medium entropy alloys [20]. Among the electrodeposited W-containing alloys with graphene, most of the effort has been devoted into Ni–W coatings [21–23]. To the best of the author's knowledge, the deposition of Fe-W-graphene composite coatings has not been studied.

Within the different graphenaceous compounds, GO is commonly employed for the electrodeposition of graphene-containing coatings. In fact, one of the main advantages of GO is its dispersibility in water and other organic solvents [24] due to the electrostatic repulsion of negatively charged oxygen-functional groups (i.e., carboxylic and phenolic hydroxyl groups) on GO surface, which facilitate its dispersion in aqueous solutions and thus its co-deposition. However, the mixture of GO with metal salt precursors will shield the charges among the charged groups on GO, and results in agglomeration of GO nanosheets. To solve this issue, various surfactants are commonly added into the electrolyte to tune the surface charge of GO and to uniformly disperse the GO sheets in the electrolyte [25]. Among the available anion surfactants, Sodium Dodecyl Sulfate (SDS) is widely used, as indicated by several publications [19,26,27]. Other works reported the use of cationic surfactants, e.g. Cetyl Trimethyl Ammonium Bromide (CTAB) for the electrodeposition of GO-containing coatings [28,29]. The use of a cationic surfactant should give the GO sheets a positive charge and therefore facilitate their deposition onto the surface of the cathode. So far, only limited number of surfactants for graphene based composite coatings have been studied, and the influence of these surfactants on graphene oxide dispersion and coating performance is not yet clear.

The aim of this work is to electrodeposit Fe-W-GO coatings with various GO concentrations and to study the effect of graphene on the microstructure, hardness and on the corrosion resistance of the composites. The effect of different surfactants (i.e., anionic, cationic, and nonionic) in facilitating GO dispersion in the electrolyte is also analyzed. The effect of different surfactants (i.e., anionic, cationic, and non-ionic) in facilitating GO dispersion in the electrolyte is also analyzed.

2. Experimental

2.1. Electrolyte preparation and characterization

The electrodeposition of the Fe-W-GO composite was performed from a Fe-W base electrolyte with the following composition: 1 M glycolic acid, 0.3 M citric acid, 0.1 M $Fe_2(SO_4)_3$ and 0.3 M Na_2WO_4. Prior to the addition of the GO and of the coating's deposition, the pH of the electrolyte was adjusted to 6.5 with the addition of NaOH. The composition of the electrolyte was selected according to the results obtained and described in previous works [6,8]. Seven different surfactants were added in the electrolyte to analyze the GO dispersion: Polydiallyldimethylammonium chloride (PDDA), Polyethylenimine (PEI), Cetrimonium bromide (CTAB), Sorbitan monooleate (Tween), 2-[4-(2,4,4-trimethylpentan-2-yl) phenoxy]ethanol (Triton), Sodium dodecyl sulfate (SDS) and sodium dodecylbenzenesulfonate (SDBS). A commercially available GO (Grafenea) was used for the deposition of the composite coatings. Prior to add the GO in the electrolyte, the GO oxide was diluted in distilled water (2 to 10 times dilution) and sonicated for one hour in order to favor the exfoliation of the graphene sheets. The GO was then added in the electrolyte in different concentrations as specified in Table 1. Zeta potential measurements on the different electrolytes containing the additives and GO were performed by Zetasizer nano (Malvern, UK) with 3 sets of repeats for each measuremnet. The electrodeposition was performed in galvanostatic mode in a two-electrode cell, using 1 cm^2 copper substrates and a Pt counter electrode. The copper substrates were degreased using a 10 M NaOH alkaline solution and then activated in 2 M H_2SO_4 solution. A nickel seed layer was deposited from a commercial chloride bath to improve the adhesion of the coating with the substrate, and the deposition was performed at 60 ℃, 10 mA/cm^2 and for 2 min. The FeW-GO coatings were deposited using the same deposition parameters, listed in Table 1, as in our previous published work [2]. The deposition time was selected accordingly to obtain 10–15 μm thick coatings. The current efficiency (CE) of the FeW-PDDA-GO coatings was calculated based on the elemental composition of the metallic elements (i.e., Fe and W) in the coatings using the Faradaýs Law, as described elsewhere [6]:

$$CE = \frac{massofdeposit}{thoreticalmass} = \frac{w^*F}{Q}\sum\frac{C_x{}^*N_x}{M_x} \quad (1)$$

where w is the mass of the deposit (g), F is Faraday's constant (96,485C•mol^{-1}), Q is the electric charge (C), C_x (x = Fe and W) is the weight fraction of each element, N_x is the ionic valence and Mx is the atomic mass (g•mol^{-3}).

2.2. Coating characterization

A Zeiss Gemini 450 (Zeiss, Oberkochen, Germany) was used to analyze the surface morphology and the cross-section of the composite coatings. The composition of the coatings was measured along the cross-section of the samples by Energy Dispersive X-ray Spectroscopy (EDS). Heat treatments were performed in the furnace of a NETZSCH 402C dilatometer, keeping the sample at 400 ℃ for 1 h under high purity Ar 6.0 atmosphere. The annealing temperature was reached with a heating rate of 10 ℃/min. After the heat treatments, the samples were kept inside the furnace until reaching room temperature. The microstructure of the as-deposited and annealed coatings was examined by X-rays diffraction (XRD) analysis performed using a Bruker D8 Discover and by EBSD analysis performed with Simmetry S2 detector. The hardness of the coatings was measured from the polished cross-section of the composite coatings using a Struers DuraScan-70 G5 Hardeness tester. For each sample, the hardness was averaged over at a minimum of fifteen HV0.005 indentations. The corrosion resistance was studied in a 0.1 M NaCl aqueous solution using a three-electrode configuration Biologic SP-300 potentiostat with a Pt counter electrode and an $Ag/AgCl/NaCl_{(3M)}$ as reference electrode. The potentiodynamic polarization measurements were performed from −1 to 0 V with a scan rate of 1 mVs^{-1}.

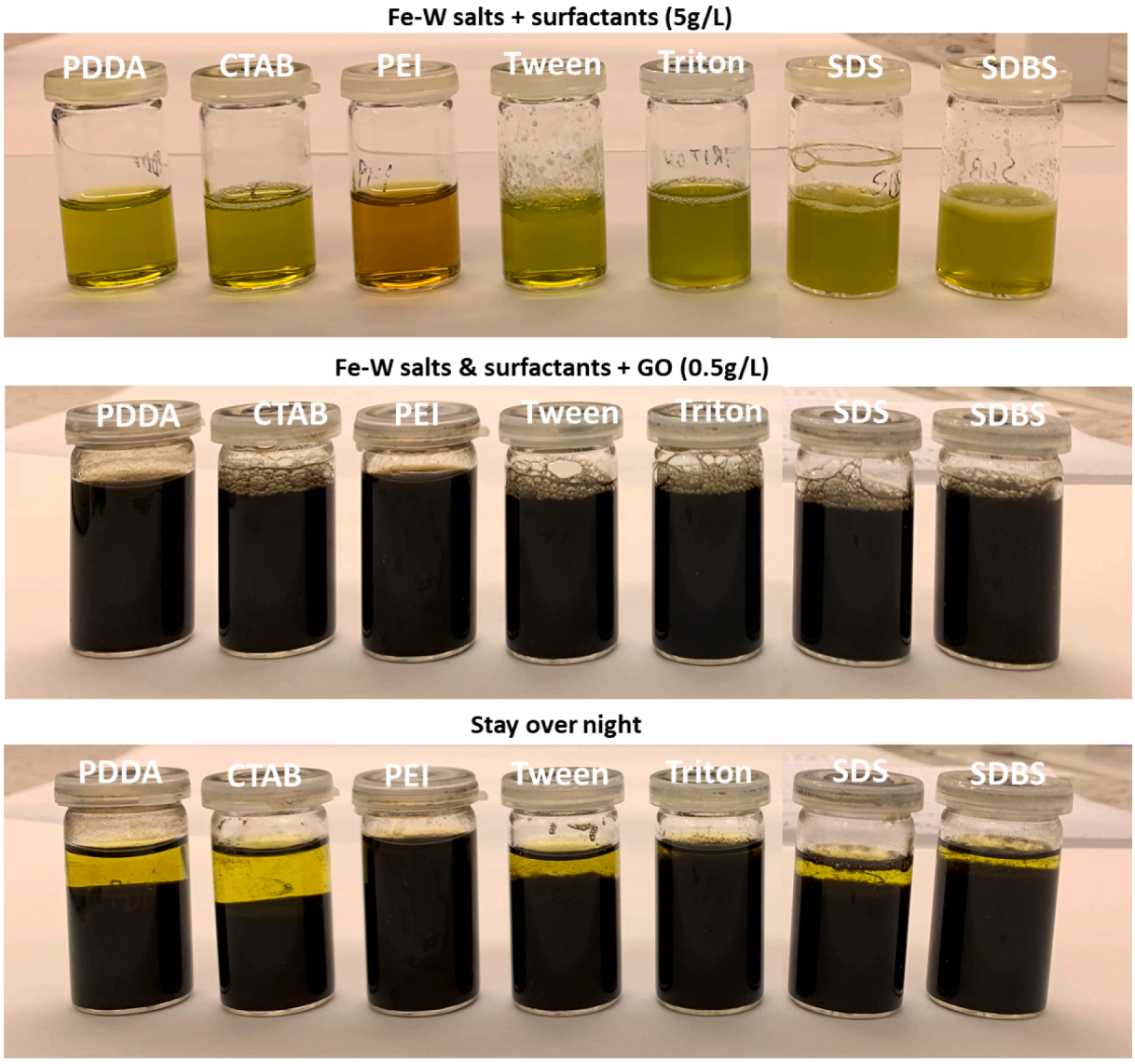

Fig. 1. Fe-W electrolytes with the addition of 5 g/L of different surfactants and with the addition of 0.5 g/L of GO. The stability of the solution was examined overnight.

Table 3
Zeta potential and average particle size of GO in different electrolytes and surfactants.

Solution	Zeta potential (mV)	Particle Z-average size (nm)
GO	−16,5 ± 3,6	1192 ± 55 nm
FeW-PDDA-GO	19,9 ± 4,47	1867 ± 77
FeW-CTAB-GO	−5,73 ± 0,51	14980 ± 1296
FeW-PEI-GO	−10,41 ± 0,87	18133 ± 3106
FeW-Tween-GO	−7,15 ± 0,93	4266 ± 410
FeW-Triton-GO	−8,58 ± 0,77	5129 ± 1435
FeW-SDS-GO	−19,60 ± 0,45	2255 ± 142
FeW-SDBS-GO	−26,17 ± 1,19	3647 ± 409

Table 4
Fe-W-GO composite coatings deposited from electrolytes containing various amounts of PDDA and GO.

PDDA GO	1 g/L	2.5 g/L	5 g/L
0 g/L	**FeW1**	**FeW2.5**	FeW5
0.1 g/L	**FeW1-0.1GO**	**FeW2.5–0.1GO**	**FeW5-0.1GO**
0.5 g/L	FeW1-0.5GO	FeW2.5–0.5GO	**FeW5-0.5GO**
1 g/L	/	/	**FeW5-1GO**
2 g/L	/	/	FeW5-2GO

3. Results and discussions

3.1. Electrolyte stability: Influence of additives and GO content

To suppress the aggregation of GO in the Fe-W electrolyte, seven types of surfactants were added and their dispersion effect was evaluated. Amongst the studied surfactants three were cationic, i.e., PDDA, CTAB and PEI, two were anionic, i.e., SDS and SDBS, and two were non-ionic, i.e., Tween and Triton. In order to properly select the additive concentration to be used, preliminary electrodeposition tests were performed using both PDDA and SDS additives. The addition of 1 g/L of PDDA proved to be sufficient to stabilize and to deposit FeW-GO composite from an electrolyte containing 0.1 g/L of GO. To deposit composites with higher GO content (i.e., 0.5 and 1 g/L), the addition of 5 g/L of PDDA was found to be necessary. Average particle size measurements were performed to evaluate the influence of PDDA and GO

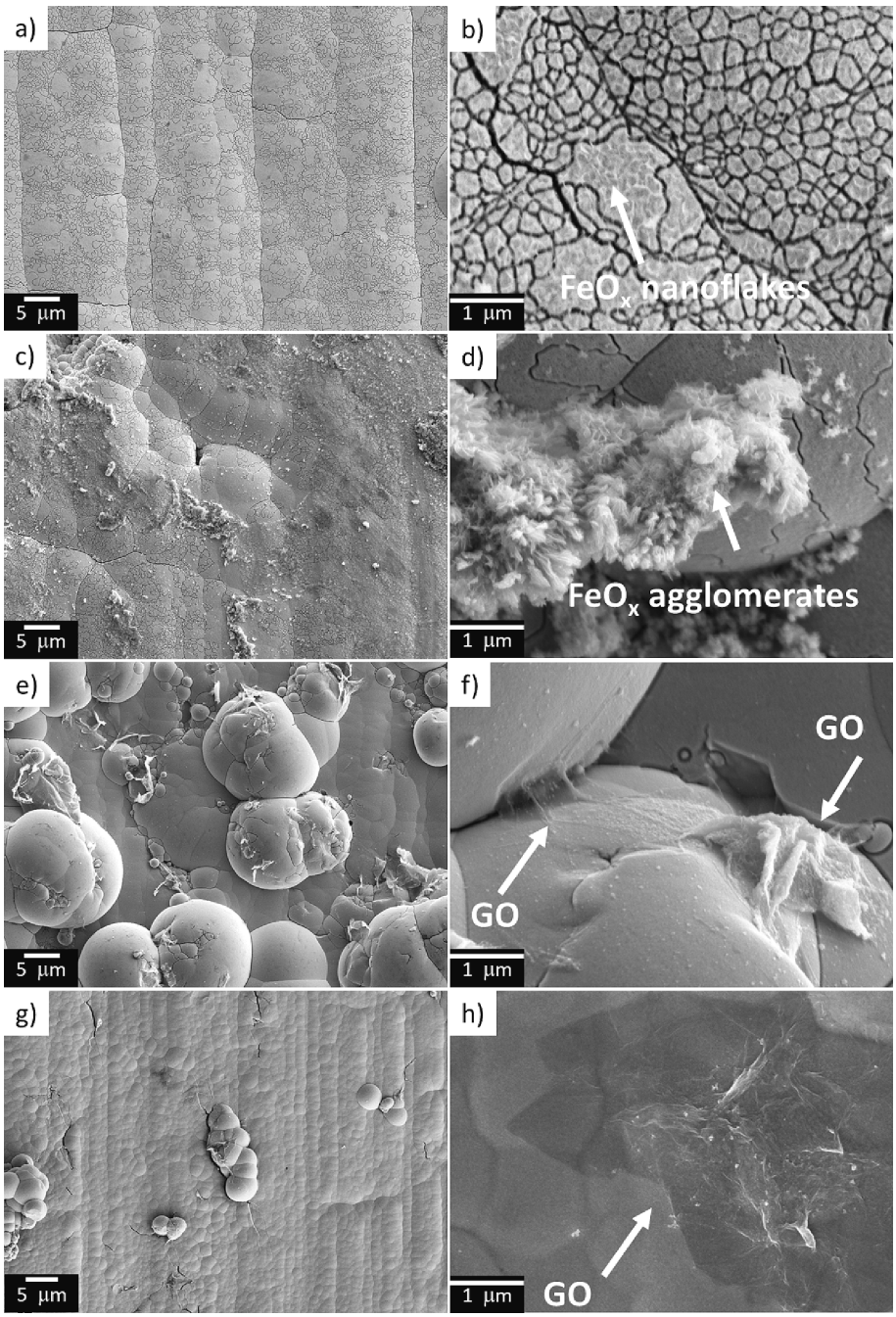

Fig. 2. SEM micrographs of the surface of the FeW (a-b), FeW5-0.1GO (c-d), FeW5-0.5GO (e-f), and FeW5-1GO (g-h) coatings.

concentration on the GO dispersibility in the electrolyte and the results of pure GO and of the GO-containing electrolytes with 1 and 5 g/L of PDDA are shown in Table 2. As Table 2 shows, an increase in PDDA from 1 to 5 g/L results in a better dispersion of GO (i.e., smaller particle size) for the electrolytes containing 0.1 and 0.5 g/L of GO. The largest particle size is measured for the FeW5PDDA-1GO electrolyte, due to the high amount of GO resulting into the agglomeration of GO sheets in solution.

On the other hand, using 1 g/L of SDS as an additive did not result in an acceptable GO dispersion in the electrolyte. Therefore, and in consideration of these findings, 5 g/L of each surfactant and 0.5 g/L of GO were added in the electrolyte to analyze the effects of the different surfactants on the GO dispersions. The mixed solutions were then monitored over time, see Fig. 1. The cationic surfactants fully dissolved in the Fe-W electrolyte. The color change of the electrolyte after the addition of PEI, as seen in Fig. 1, was related to an increase in the solution pH (from 6.5 to around 7.5). Regarding the non-ionic surfactants, Tween did not completely dissolve in the electrolyte, as shown from the solid precipitates formed on the glass vials. The same was observed for the anionic surfactant SDBS. After the addition of the surfactants, 0.5 g/L of GO was added in each solution while the electrolyte was vigorously stirred at 600 rpm. The GO-containing solutions were stable for several hours, but overnight the added GO agglomerated and precipitated in most solutions. However, a two-hour stability of the GO-containing solutions is already sufficient for the desired thickness of the composite coatings (~10 to 15 µm). To accurately evaluate the effect of the different surfactants on the GO dispersion, zeta potential and average particle size measurements were performed and the results are included in Table 3. The zeta potential indicates the magnitude of electrostatic repulsion forces between charged particles in a colloidal solution. The surfactants added in solution have the crucial role to

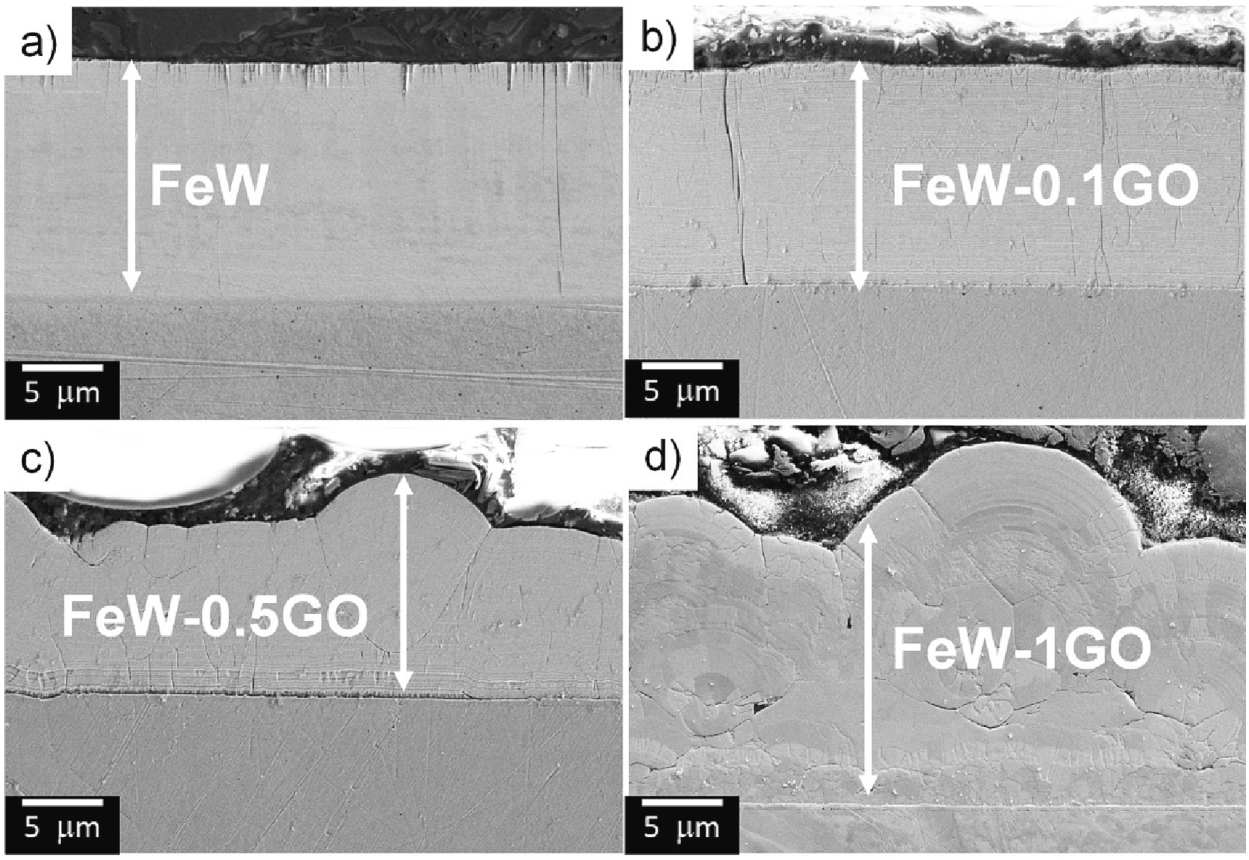

Fig. 3. SEM micrographs of the cross-section of the FeW (a), FeW5-0.1GO (b), FeW5-0.5GO (c), and FeW5-1GO (d) coatings.

Table 5
Chemical composition of composite coatings measured by EDS analysis.

Sample	Fe (at.%)	W (at.%)	O (at.%)	CE (%)
FeW1	75,9 ± 0,5	18,9 ± 0,3	5,7 ± 0,2	73%
FeW5-0.1GO	75,9 ± 2,4	18,6 ± 2,1	5,5 ± 0,3	63%
FeW5-0.5GO	74,4 ± 1,3	20,2 ± 1,3	5,4 ± 0,4	63%
FeW5-1GO	76,16 ± 1,6	18,4 ± 1,2	5,4 ± 0,8	64%

provide the GO sheets with surface charges. Hence, the resulting electrostatic repulsion forces between different GO sheets will lead to a stable GO dispersion. Generally, the absolute value of the zeta potential is used to evaluate and compare the stability of different solution: a higher absolute zeta potential value corresponds to a more stable GO dispersion [30]. Among the cationic surfactants, the addition of PDDA resulted into the highest zeta potential and the smallest particle size, i.e., 19,9 mV and 1192 nm, respectively. The non-ionic surfactants Tween and Triton are characterized with relatively similar values of zeta potentials and particles size. Finally, the addition of anionic surfactants resulted in high negative values of zeta potentials, and particles sizes in the range of 2 to 3 µm. It is worth noticing that a positive zeta potential would be expected when adding a cationic surfactant, like in the case of the PDDA containing electrolyte (see Table 3). This indicates the presence of positive charges on the surface of the GO sheets a therefore correct surfactant functionalization [31]. The slightly negative zeta potential values observed when adding the two others cationic surfactants (i.e., CTAB and PEI) indicates a lower ability to functionalize GO sheets and therefore a lower ability to stabilize the GO dispersion. This is also confirmed from the differences in the particles size: the particle size of electrolytes containing CTAB-GO and PEI-GO is more than 10 times higher as compared to the PDDA-GO electrolyte. Among the studied surfactants, the results in Table 3 indicate that the use of PDDA results

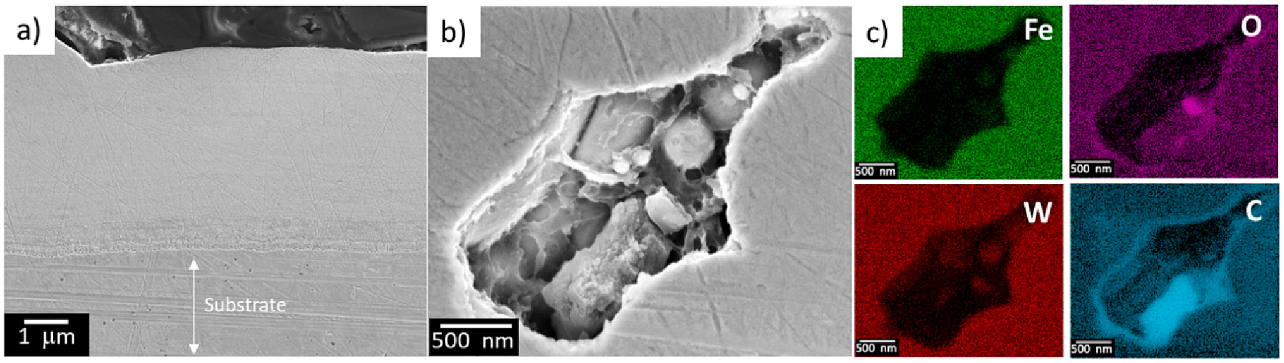

Fig. 4. SEM micrographs (a-b) acquired from the cross-section of the FeW5-05GO sample and EDS elemental maps acquired from the area shown in (b).

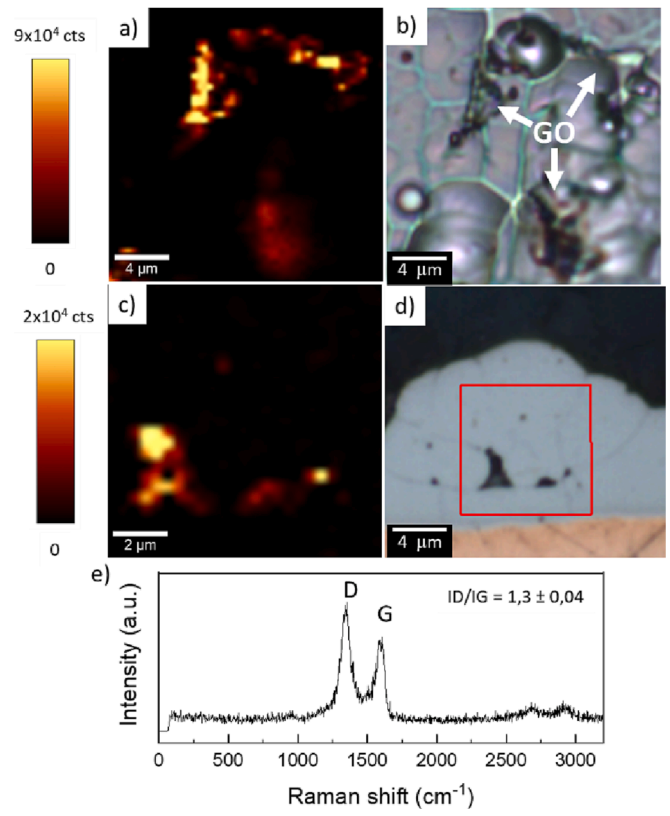

Fig. 5. Raman mapping of the surface (a-b) and cross-section (c-d) of the FeW5-05GO coating. G band intensity maps are shown in (a) and (c), whereas the respective acquisition sites are shown in (b) and (d). A representative Raman spectrum acquired from the coating is shown in (e).

into the best GO dispersions: high absolute value of zeta potential and smallest particle size. In fact, the average particle size measured for the FeW-PDDA-GO electrolyte and for pure GO is in the same order of magnitude (see Table 3), indicating only minimal GO agglomeration. In consideration of the zeta potential results, electrodeposition trials were also performed selecting one additive of each type (i.e., cationic, anionic and non-ionic): (i) PDDA, (ii) Triton and (iii) SDS. Having SDS and SDBS relatively similar zeta potentials and particles size values, SDS was preferred thanks to its higher solubility in the electrolyte (see Fig. 1). A test sample of Fe-W-GO composite was then electrodeposited using the selected additives and 0.5 g/L of GO with the electrodeposition conditions as specified in Table 1. To ensure that the required composite thickness was achieved, the deposited specimen was weighed, and the surface appearance examined for any apparent inhomogeneities in the surface morphology (see Fig. S1 in the supportive information). From the obtained results of the zeta potentials measurements of the electrodeposition trials, PDDA was selected as the most promising surfactant and used to deposit composite coatings from electrolytes containing different concentrations of both surfactant and GO. The deposited composite coatings are specified in Table 4. The samples that met the thickness and appearance requirements described above are highlighted in bold in Table 4. In the following paragraphs are included the results from the characterization of the coatings deposited with 5 g/L of PDDA and with increasing GO content. The hardness results from the coating deposited with 1 and 2.5 g/L of PDDA are included in the supportive information. The same nomenclature as in Table 4 will be used in the following.

3.2. Structural characterization of FeW-GO coatings

The surface morphology of the FeW and FeW-GO coatings was analyzed by use of SEM and the results are shown in Fig. 2. The images of the polished cross-sections are shown in Fig. 3. The surface of the FeW coatings appears smooth with some superficial cracks, see Fig. 2a-b. Such cracks can be considered superficial since they are only found down to a depth of ~ 1 µm from the surface of the coatings. The presence of such cracks can be related to the high amount of co-deposited W in the coating: high W concentrations are leading to an increase of internal stresses in the coatings [32]. The chemical composition of the coatings was measured by EDS analysis performed along the cross-sections of the coatings. The results from the chemical analysis and of the CE of the deposited coatings are provided in Table 5. As shown in Table 5, the

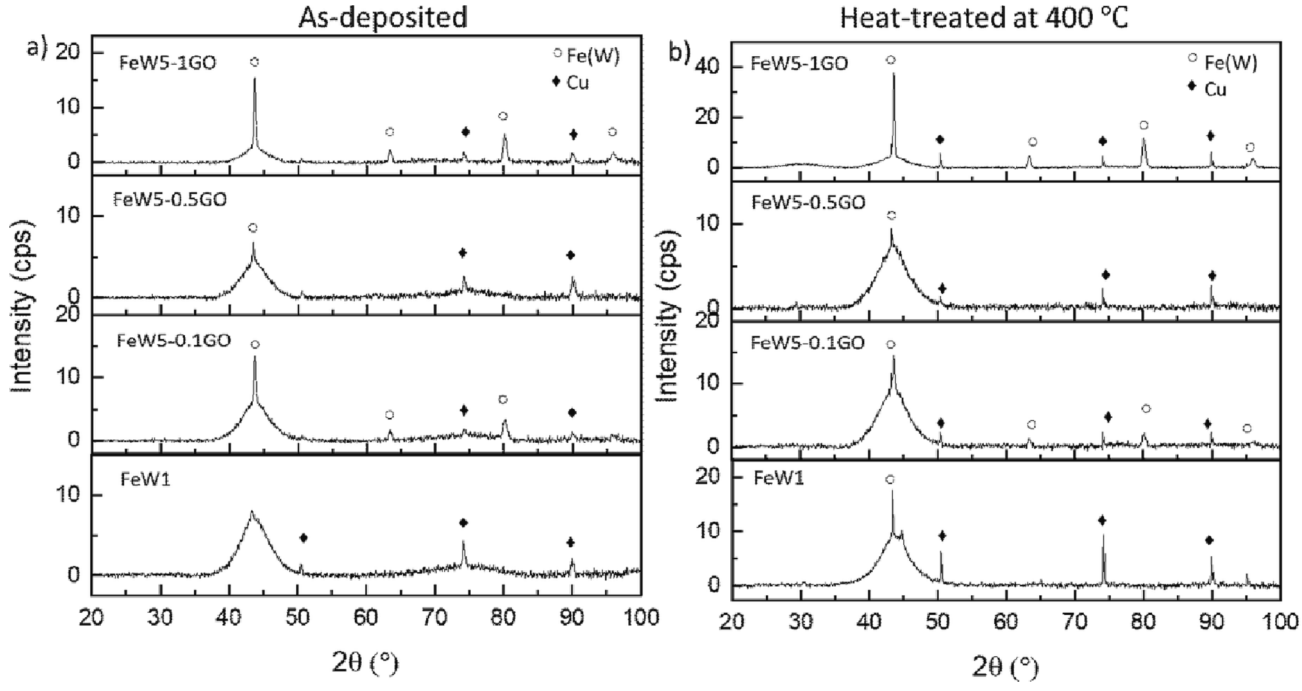

Fig. 6. XRD spectra of the FeW and FeW-GO coating in as-deposited condition (a) and after heat treatment (b).

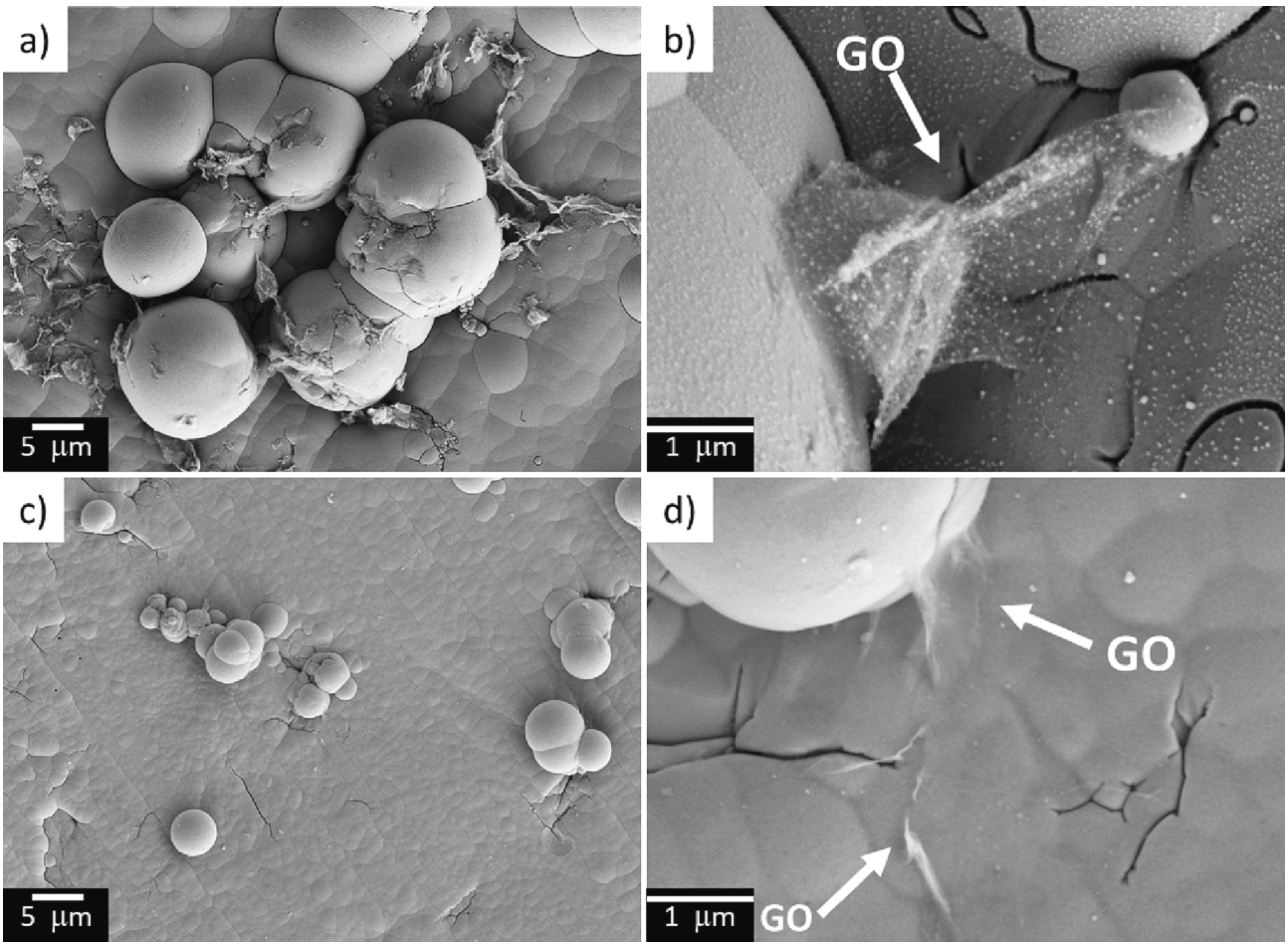

Fig. 7. SEM micrographs of the surface of the heat-treated FeW5-0.5GO (a-b) and FeW5-1GO (c-d). White arrows are added in (b) and (d) to mark the presence of GO sheets.

highest CE is observed for the deposition of the GO-free coating whereas only a minor difference of the CE is observed when increasing the GO quantity from 0.1 g/L to 1 g/L. Such decrease in CE for the deposition of GO-containing coatings can be explained considering the lower conductivity of the GO as compared to the metallic elements.

The surface of the FeW5-0.1GO coating looks similar to the FeW coatings as the presence of GO is not clearly observed (Fig. 2c). It is observed that surface oxides form clusters several micrometers in size, see Fig. 2d. A partially globular topography is observed for the FeW5-0.5GO and FeW5-1GO coatings. In addition, GO sheets can be clearly observed along the surface of the coatings, see Fig. 2e-h (for clarity, the location of some GOs is highlighted with arrows). As shown from the SEM images, GO sheets are deposited with different thicknesses: extremely thin (i.e., electron transparent) and as stacks of several layers see Fig. 2f and Fig. 2h.

As seen in Figs. 3 and 4a, GO sheets are not visible in the polished cross-sections of the dense and uniform metallic matrix. However, as Fig. 4b shows few cavities are found throughout the cross-section of the composites. Inside such cavities, it is possible to observe thin sheets with a web-like structure. The observed phase can be expected to be GO: EDS analysis shows that the features are rich in C and O (see Fig. 4e-f). However, due to possible presence of other carbon-based impurities EDS analyses cannot be solely used to determine the presence of graphene in the coatings. Therefore, Raman mapping was performed both on the surface and along the cross-sections of the composite coatings to confirm the presence of GOs. Fig. 5a shows the G band intensity map acquired from the surface of the FeW5-0.5GO coating (shown in Fig. 5b), whereas Fig. 5c shows the G band intensity map acquired from the coatings cross-section (shown in Fig. 5d). A representative Raman spectrum acquired from the bright areas in the G band intensity maps is shown in Fig. 5e. The results clearly show that the Raman spectrum collected from the composite coatings is characterized with two distinctive peaks expected from GO: the D band peak at 1350 cm^{-1} and the G band peak at 1579 cm^{-1} [33]. The G peak relates to stretching of the sp^2 hybridized carbon bonds, whereas the D peak is due to the incorporation of defects (e.g. substitutional atoms like oxygen) in the hexagonal carbon lattice [34]. The average ratio of the intensities of the D and G peaks (i.e., ID/IG) can give a good indication of defectiveness in graphene-related materials [33] and it is therefore shown in Fig. 5e. The G band intensity maps highlight the variation in the intensity of the G band as a function of spatial location: bright areas in the map are indicating the presence of GO. Therefore, the Raman results shown in Fig. 5 confirm that the observed C-rich phases observed on the surface and along the cross-section of the FeW-GO coatings are GOs.

The composite coatings were subjected to heat treatments for one hour at 400 ℃ in order to study the thermal stability of the co-deposited GO within the coatings. Fig. 6 shows the XRD results of the coatings before and after the thermal treatment. The FeW coating deposited without graphene has an amorphous structure, as shown by the broad XRD shoulder between 40 and 50 in Fig. 6. The amorphous structure is a result of the high amount of co-deposited W as previously shown for coatings with similar composition [8]. Both the FeW5-0.1GO and FeW5-0.5GO coatings show a slight increase in the crystallinity of the FeW matrixes, as seen from the presence of a small Fe(W) peak in Fig. 6a.

The chemical composition of the coatings is almost identical, see Table 5, therefore it can be assumed that the addition of GO resulted in a

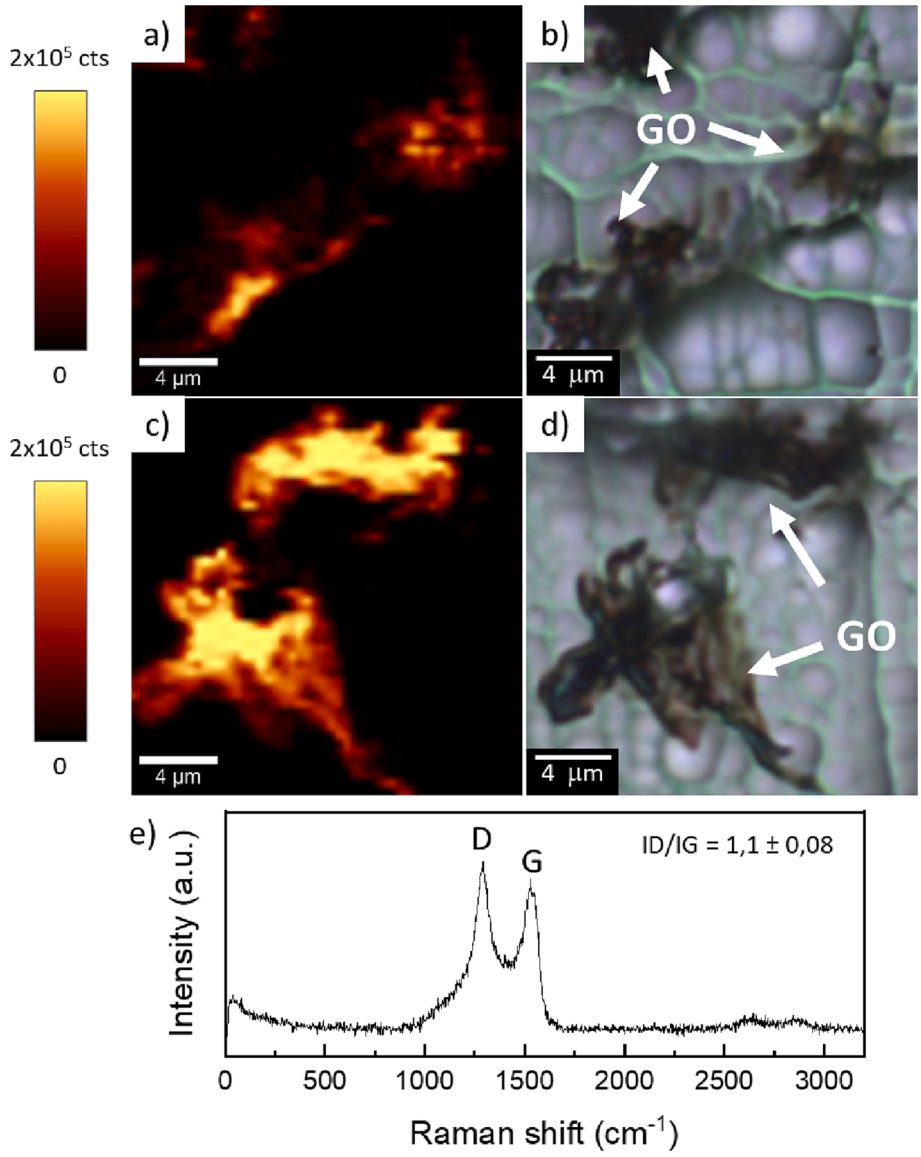

Fig. 8. Raman mapping of the surface (a-b) and cross-section (c-d) of the heat-treated FeW5-0.5GO coating. G band intensity maps are shown in (a) and (c), whereas the respective acquisition sites are shown in (b) and (d). A representative Raman spectrum acquired from the coating is shown in (e).

crystallinity increase of the metallic matrix. The co-deposited GO sheets can act as nucleation sites for the electrocristallization of FeW grains [19], which would then increase the amount of crystalline grains. The increase in crystallinity is even more evident in the FeW5-1GO sample, see Fig. 6a. After the heat treatment at 400 ℃, only minor microstructural changes are observed. An increase in the crystallinity of the coatings is found: the crystalline peaks appear sharper and have a higher intensity. This is especially evident for the FeW5-1GO sample, where the intensity of the Fe(W) peaks after the heat treatment is more than two times higher as compared to the as-deposited sample. Yet, the structure of the FeW, FeW5-0.1GO and FeW5-0.5GO coatings is still largely amorphous. The slight changes after the heat treatments are related to the excellent thermal stability of FeW coatings that are W-rich (i.e., over 20 at.%). Previous studies have shown that much of the deposited amorphous structure is retained even after heat treatment at 800 °C [35]. After the heat treatment, GO was retained in the composite coatings, as shown in the SEM analyses in Fig. 7 and in the Raman mapping shown in Fig. 8 where GOs are marked by arrows.

3.3. Mechanical properties and corrosion resistance of Fe-W-GO coatings

To analyze the influence of GO on the hardness of the composite coatings, hardness measurements were performed on the as-deposited and heat-treated samples and the results are shown in Fig. 9. In the as-deposited composites, the co-deposition of GO leads to a progressive increase of the hardness, with the maximum value of 1150,3 HV measured for the FeW5-1GO coating. Considering that the composition and the microstructure of the FeW matrices are almost identical (especially for the FeW, FeW5-0.1GO and FeW5-0.5GO coatings), the observed increase in hardness can be attributed to the influence of GO. Furthermore, the hardness of the as-deposited coatings with different PDDA and GO content was also evaluated to exclude the influence on the hardness of the PDDA surfactant (see Fig. S2 in the supportive information). In the pure FeW coatings it is observed only a limited variation in the hardness with the increasing of PDDA quantity (~7% decrease in the hardness when adding up to 2.5 g/L of PDDA). Therefore, the observed increase in the hardness when adding GO can only be attributed to the effects of GO co-deposition. As already described in several previous research studies, the strengthening effect provided by GO can

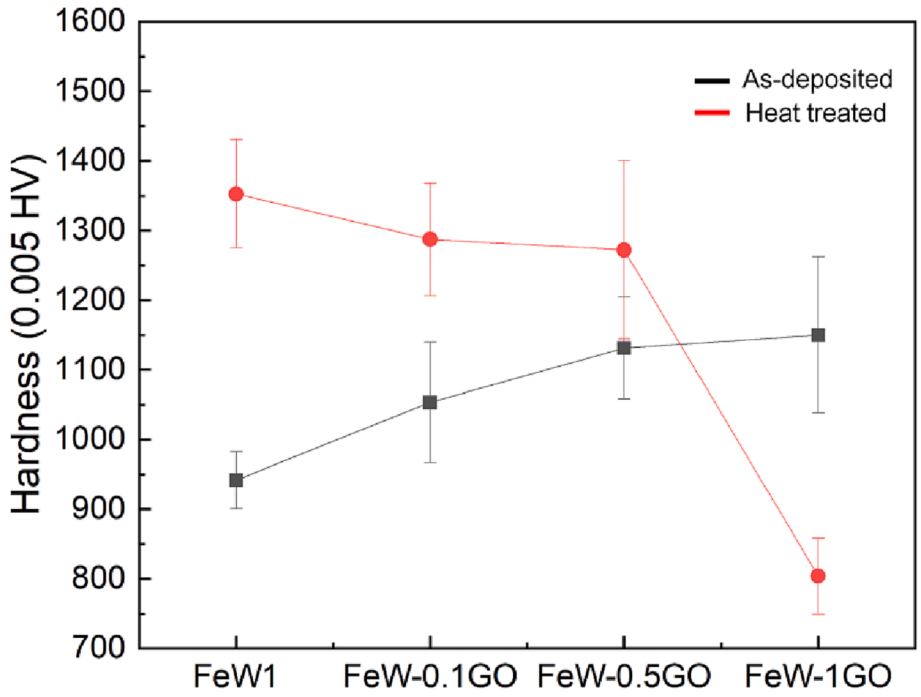

Fig. 9. Hardness of the as-deposited and heat-treated FeW and FeW-GO coatings.

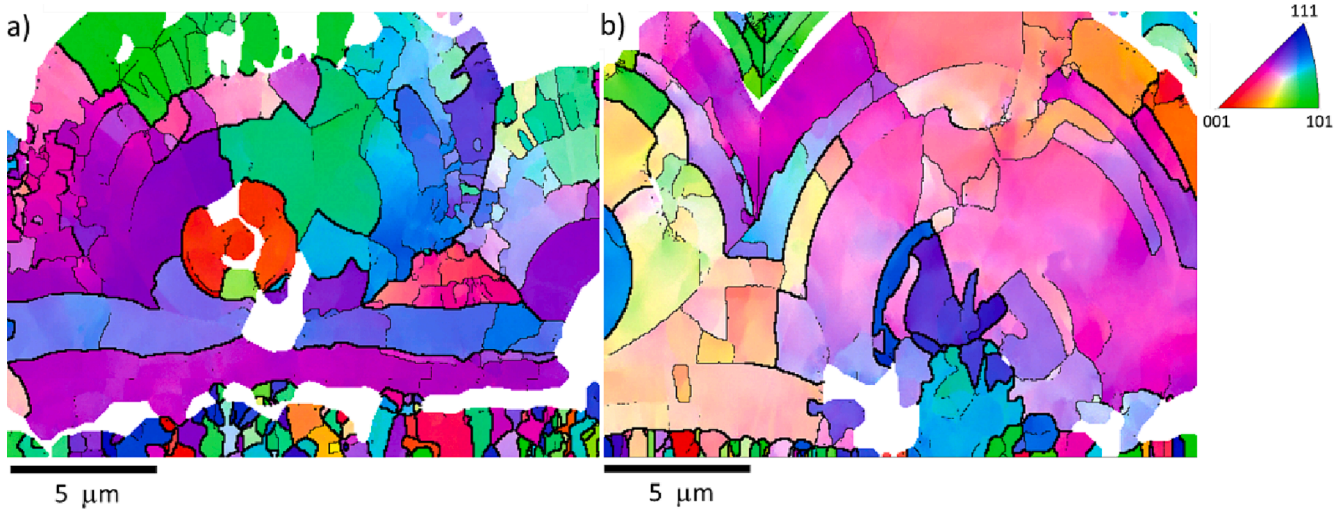

Fig. 10. EBSD orientation map in inverse pole figure coloring along the growth direction of the as-deposited FeW5-1GO (a) and of the heat-treated (1 h at 400 °C) FeW5-1GO (b) coatings.

be ascribed to load transfer [26] and the inherent high mechanical strength of graphene [36]. After the heat treatment an increase in the hardness is observed for the pure FeW, FeW5-0.1GO and FeW5-0.5GO samples. Such increase in the hardness of the samples can be related to the microstructural changes occurring in the amorphous FeW matrixes when annealing at 400 ℃. The formation of nanometric Fe-rich grains in the amorphous matrix can be hold responsible for the hardness increase, as shown in a previous study [10]. In the case of the FeW5-1GO sample the as-deposited structure is already largely crystalline, see XRD results in Fig. 6a. Therefore, the above-mentioned precipitation strengthening mechanism is not occurring. The observed decrease in hardness can probably be attributed to grain growth mechanisms and to increased crystallinity. To confirm such hypothesis EBSD analyses were performed on the as-deposited and annealed FeW5-1GO samples, and the acquired EBSD orientation maps are shown in Fig. 10. As can be seen in Fig. 10, the structure of the as-deposited FeW5-1GO sample is characterized by small equiaxed grains in the proximity of the substrate and by larger grains forming a globular structure, as already observed in Fig. 2. The sample has a random texture, as there is no prevalent orientation in both inverse pole figure maps. After the heat treatment at 400 ℃, only small differences can be observed in the structure of the coating. A reduction in the amount of small and equiaxed grains and also a reduced amount of low angle grain boundaries (i.e., $3° < x < 10°$) within the larger globular grains can be observed, whereas no evident difference in grain size is observed. Hence, the increase in crystallinity after the heat treatment, as revealed from the XRD results, could explain the decrease in hardness. Also, it can be hypothesized that the high loading of GO in the FeW5-1GO is more affected by the annealing process. A partial thermal reduction of the GO during the annealing treatment would result in the evaporation of adsorbed water and gasses

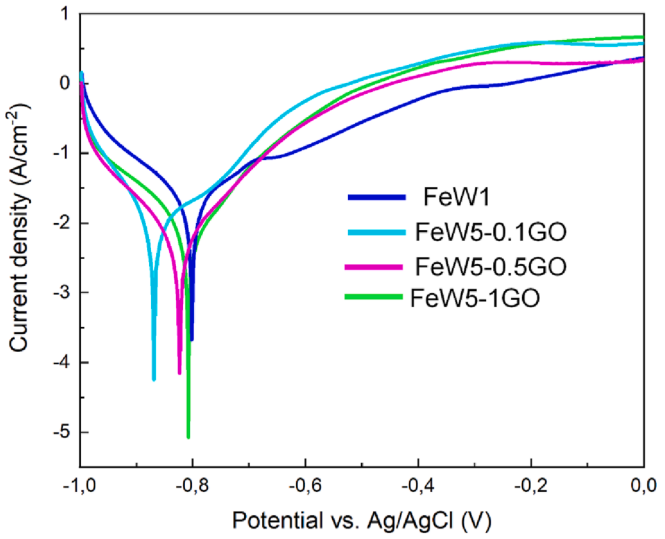

Fig. 11. Polarization curves of the FeW and FeW-GO coatings measured in 0.1 M NaCl solution.

Table 6
Corrosion parameters.

Sample	-Ecorr, V	-jcorr, μA/cm^2	βc (V)	βa (V)
FeW1	0,8	29,4	0,15	0,28
FeW5-0.1GO	0,87	7,8	0,07	0,15
FeW5-0.5GO	0,82	5,7	0,13	0,11
FeW5-1GO	0,81	8,5	0,21	0,15

releases (e.g. CO, CO_2, H_2 etc.). This would result in the formation of small voids and therefore into a worse bonding between the metallic matrix and the GOs.

The corrosion resistance of the composite coatings was studied using a 0.1 M NaCl solution and the measured polarization curves are shown in Fig. 11 whereas the extracted corrosion parameters are listed in Table 6. A large decrease in corrosion current density (i.e., ~80 %) is observed for all graphene-containing coatings compared to the pure FeW coating, see Table 6. The lowest corrosion current density of 5,7 μA/cm^2 was measured for the FeW5-05GO composite. A slightly lower corrosion potential is also measured for the composites. Usually, a lower corrosion potential indicates a higher tendency of the sample to corrode. However, the hydrogen overvoltage on the FeW surface can vary with different amounts of GO without there being a direct correlation with the corrosion rate [11]. In addition, previous corrosion studies on graphene-containing coatings have shown a similar negative shift in the corrosion potential of the coatings, which were still characterized by a lower corrosion current compared to the graphene-free coating [21,37]. With regards to the corrosion mechanism of the Fe-W-GO coatings, galvanic corrosion should also be considered. As shown in the cross-section SEM micrographs, the co-depositions of GO resulted in the formations of cavities and cracks that could extend until the Ni seed layer. The electrolyte passing through the cracks could reach the Ni layer initiating galvanic corrosion with the Fe matrix. Furthermore, GO itself is cathodic with respect to Fe and can result into galvanic corrosion with Fe [38]. This could explain the slight increase in corrosion current observed for the FeW5-1GO sample as compared to the other two samples deposited with lower amounts of GO, see Table 6. Despite such slight increase in the corrosion current for the FeW5-1GO sample, the corrosion current of the GO-containing coatings is much lower as compared to the FeW coating. Therefore, similar to what was said earlier regarding the hardness increase, the observed increase in corrosion resistance can be related to the incorporation of graphene into the coatings, considering the very similar composition and structure between the graphene-containing and the pure FeW coatings. In particular, the well-dispersed graphene on the surface of the coatings act as a barrier to the penetration of the corrosive media and improving the overall corrosion resistance of the coating [19].

4. Summary and conclusions

In this work, graphene-containing Fe-W coatings were electrodeposited from a glycolate-citrate electrolyte and graphene oxide in various concentration. Among the additives tested to stabilize the graphene oxide in the electrolyte, PDDA was selected and used to deposit the FeW-GO composite coatings with 0.1, 0.5 and 1 g/L of GO. The composition and structure of the composite coatings were studied using SEM, XRD and EBSD technique. Raman analyses were used to determine the presence of graphene in the deposited coatings. The coatings were also subjected to a 1 h heat treatment at 400 ℃ to investigate its influence on the co-deposited graphene and on the hardness of the composites. Finally, the influence of the graphene on the corrosion resistance of the coatings was also studied. From the results obtained in this work, the following conclusion can be drawn:

- The addition of 5 g/L of PDDA proved to be effective for the stabilization of GO in the FeW electrolytes and for the deposition of FeW-graphene composite with an increasing amount of GO: 0.1, 0.5 and 1 g/L. Lower amount of PDDA could also be used to successfully deposit composite coatings with 0.1 g/L of GO.
- Raman mapping and SEM analysis confirmed the successful co-deposition of graphene on the surface and along the cross-section of the coatings. The graphene in the coatings was retained even after a 1 h heat treatment at 400 ℃.
- The addition of graphene did not alter the composition of the FeW matrices while the structure of the coatings was minimally changed. As compared to the amorphous structure of the graphene-free coatings, a slight increase in crystallinity was observed in the FeW5-0.1GO and FeW5-05GO coatings, whereas a crystalline structure was observed for the FeW5-1GO.
- The addition of graphene led to an improvement in the hardness of all the graphene-containing coatings. In the case of the FeW5-0.1GO and FeW5-0.5GO coatings, the hardness could be further improved due to the precipitation hardening of the amorphous FeW matrices by the heat treatment. A decrease in the hardness was observed in the heat-treated FeW5-1GO due to grain growth and stress relaxation in the crystalline FeW matrix.
- The addition of graphene also significantly improved the corrosion resistance of the composite coatings, with a maximum of 81% decrease in the corrosion current density measured for the FeW5-0.5GO coating.

Declaration of Competing Interest

The authors declare that they have no known competing financial interests or personal relationships that could have appeared to influence the work reported in this paper.

Data availability

Data will be made available on request.

Acknowledgements

The research leading to these results has received funding from Chalmers Foundation.

Appendix A. Supplementary data

Supplementary data to this article can be found online at https://doi.org/10.1016/j.flatc.2023.100525.

References

[1] A. Mulone, J. Hildenbrand, U. Klement, Electrodeposition: three steps towards sustainability, Trans. Inst. Met. Finish. 98 (2020) 108–113, https://doi.org/10.1080/00202967.2020.1748344.

[2] A. Mulone, A. Nicolenco, N. Imaz, J. Fornel, J. Sort, U. Klement, Effect of heat treatments on the mechanical and tribological properties of electrodeposited Fe–W/Al2O3 composites, Wear. (2020) 448–449, https://doi.org/10.1166/sam.2018.3304.

[3] G.A. Lausmann, Electrolytically deposited hardchrome, Surf. Coatings Technol. 86–87 (1996) 814–820, https://doi.org/10.1016/S0257-8972(96)02973-8.

[4] J.M. Tyler, Automotive applications for chromium, Met. Finish. 93 (10) (1995) 11–14.

[5] F. Pierre, F. Diebold, F. Baruthio, Biomonitoring of two types of chromium exposure in an electroplating shop, Int. Arch. Occup. Environ. Heal. 81 (3) (2007) 321–329.

[6] A. Nicolenco, N. Tsyntsaru, H. Cesiulis, Fe (III)-Based Ammonia-Free Bath for Electrodeposition of Fe-W Alloys, J. Electrochem. Soc. 164 (2017) D590–D596, https://doi.org/10.1149/2.1001709jes.

[7] A. Nicolenco, N. Tsyntsaru, J. Fornell, E. Pellicer, J. Reklaitis, D. Baltrunas, H. Cesiulis, J. Sort, Mapping of magnetic and mechanical properties of Fe-W alloys electrodeposited from Fe(III)-based glycolate-citrate bath, Mater. Des. 139 (2018) 429–438, https://doi.org/10.1016/j.matdes.2017.11.011.

[8] A. Mulone, A. Nicolenco, V. Hoffmann, U. Klement, N. Tsyntsaru, H. Cesiulis, In-depth characterization of as-deposited and annealed Fe-W coatings electrodeposited from glycolate-citrate plating bath, Electrochim. Acta. 261 (2018) 167–177, https://doi.org/10.1016/j.electacta.2017.12.051.

[9] A. Mulone, A. Nicolenco, J. Fornell, E. Pellicer, N. Tsyntsaru, H. Cesiulis, J. Sort, U. Klement, Enhanced mechanical properties and microstructural modifications in electrodeposited Fe-W alloys through controlled heat treatments, Surf. Coatings Technol. 350 (2018) 20–30, https://doi.org/10.1016/j.surfcoat.2018.07.007.

[10] A. Mulone, I. Ennen, A. Hütten, U. Klement, In-situ TEM annealing of amorphous Fe-24at.%W coatings and the effect of crystallization on hardness, J. Mater. Sci. 56 (2021) 4006–4012, https://doi.org/10.1007/s10853-020-05485-7.

[11] A. Nicolenco, A. Mulone, N. Imaz, N. Tsyntsaru, J. Sort, E. Pellicer, U. Klement, H. Cesiulis, E. García-Lecina, Nanocrystalline Electrodeposited Fe-W/Al2O3 Composites: Effect of Alumina Sub-microparticles on the Mechanical, Tribological, and Corrosion Properties, Front. Chem. 7 (2019) 241, https://doi.org/10.3389/fchem.2019.00241.

[12] S. Zhou, Y. Wu, W. Zhao, J. Yu, F. Jiang, Y. Wu, L. Ma, Designing reduced graphene oxide/zinc rich epoxy composite coatings for improving the anticorrosion performance of carbon steel substrate, Mater. Des. 169 (2019), 107694, https://doi.org/10.1016/j.matdes.2019.107694.

[13] D.G. Papageorgiou, I.A. Kinloch, R.J. Young, Mechanical properties of graphene and graphene-based nanocomposites, Prog. Mater. Sci. 90 (2017) 75–127, https://doi.org/10.1016/J.PMATSCI.2017.07.004.

[14] J.H. Lee, S.J. Park, J.W. Choi, Electrical property of graphene and its application to electrochemical biosensing, Nanomaterials. 9 (2019), https://doi.org/10.3390/nano9020297.

[15] E. Pop, V. Varshney, A.K. Roy, Thermal properties of graphene: Fundamentals and applications, MRS Bull. 37 (2012) 1273–1281, https://doi.org/10.1557/mrs.2012.203.

[16] S.-M. Choi, H. Awaji, Nanocomposites-a new material design concept, Sci. Technol. Adv. Mater. 6 (2004) 2–10, https://doi.org/10.1016/j.stam.2004.06.002.

[17] C.L.P. Pavithra, B.V. Sarada, K.V. Rajulapati, T.N. Rao, G. Sundararajan, A new electrochemical approach for the synthesis of copper-graphene nanocomposite foils with high hardness, Sci. Rep. 4 (2014) 1–7, https://doi.org/10.1038/srep04049.

[18] S. Singh, S. Samanta, A.K. Das, R.R. Sahoo, Tribological investigation of Ni-graphene oxide composite coating produced by pulsed electrodeposition, Surfaces and Interfaces. 12 (2018) 61–70, https://doi.org/10.1016/j.surfin.2018.05.001.

[19] S. Li, G. Song, Y. Zhang, Q. Fu, C. Pan, Graphene-Reinforced Zn-Ni Alloy Composite Coating on Iron Substrates by Pulsed Reverse Electrodeposition and Its High Corrosion Resistance, ACS Omega. 6 (2021) 13728–13741, https://doi.org/10.1021/acsomega.1c00977.

[20] A. Aliyu, C. Srivastava, Microstructure and electrochemical properties of FeNiCoCu medium entropy alloy-graphene oxide composite coatings, J. Alloys Compd. 864 (2021), 158851, https://doi.org/10.1016/j.jallcom.2021.158851.

[21] D. Cheng, L. Zhang, Z. Zhan, H. Xia, K. Ma, H. Ma, Y. Gao, Preparation and Properties of Ni–W Composite Coatings Reinforced by Graphene Nanoplatelets, Adv. Eng. Mater. 23 (2021) 1–8, https://doi.org/10.1002/adem.202001309.

[22] C.K. Sarangi, B.P. Sahu, B.K. Mishra, R. Mitra, Pulse electrodeposition and characterization of graphene oxide particle-reinforced Ni–W alloy matrix nanocomposite coatings, J. Appl. Electrochem. 50 (2020) 265–279, https://doi.org/10.1007/s10800-019-01387-y.

[23] Y. Fan, Y. He, P. Luo, T. Shi, X. Chen, Pulse Current Electrodeposition and Properties of Ni-W-GO Composite Coatings, J. Electrochem. Soc. 163 (2016) D68–D73, https://doi.org/10.1149/2.0171603jes.

[24] V.V. Neklyudov, N.R. Khafizov, I.A. Sedov, A.M. Dimiev, New insights into the solubility of graphene oxide in water and alcohols, Phys. Chem. Chem. Phys. 19 (2017) 17000–17008, https://doi.org/10.1039/c7cp02303k.

[25] Y.J. Mai, M.P. Zhou, H.J. Ling, F.X. Chen, W.Q. Lian, X.H. Jie, Surfactant-free electrodeposition of reduced graphene oxide/copper composite coatings with enhanced wear resistance, Appl. Surf. Sci. 433 (2018) 232–239, https://doi.org/10.1016/j.apsusc.2017.10.014.

[26] T. Van Hau, A. Pham, V. Trinh, N. Phuong, H. Nam, N. Van Tu, V.D. Lam, D. D. Phuong, A. Phan, N. Minh, B.H. Thang, Electrodeposited nickel-graphene nanocomposite coating: effect of graphene nanoplatelet size on its microstructure and hardness, RSC. (2020), https://doi.org/10.1039/d0ra03776a.

[27] J. Chen, J. Li, D. Xiong, Y. He, Y. Ji, Y. Qin, Preparation and tribological behavior of Ni-graphene composite coating under room temperature, Appl. Surf. Sci. 361 (2016) 49–56, https://doi.org/10.1016/J.APSUSC.2015.11.094.

[28] M. Uysal, H. Akbulut, M. Tokur, H. Algül, T. Çetinkaya, Structural and sliding wear properties of Ag/Graphene/WC hybrid nanocomposites produced by electroless co-deposition, J. Alloys Compd. 654 (2016) 185–195, https://doi.org/10.1016/J.JALLCOM.2015.08.264.

[29] R. M. y., M.K. Punith Kumar, C. Srivastava, Electrochemical behaviour of chromium-graphene composite coating, RSC Adv. 6 (67) (2016) 62083–62090.

[30] H. Zhang, N. Zhang, F. Fang, Synergistic effect of surfactant and saccharin on dispersion and crystal refinement for electrodeposition of nanocrystalline nickel/graphene oxide composite, Surf. Coatings Technol. 402 (2020), 126292, https://doi.org/10.1016/j.surfcoat.2020.126292.

[31] H. Zhang, N. Zhang, F. Fang, Electrodeposition of Nickel/Graphene Oxide Particle Composite Coatings: Effect of Surfactants on Graphene Oxide Dispersion and Coating Performance, J. Electrochem. Soc. 167 (2020), 162501, https://doi.org/10.1149/1945-7111/ABCC32.

[32] F. He, J. Yang, T. Lei, C. Gu, Structure and properties of electrodeposited Fe-Ni-W alloys with different levels of tungsten content: A comparative study, Appl. Surf. Sci. 253 (2007) 7591–7598, https://doi.org/10.1016/j.apsusc.2007.03.068.

[33] M.S. Dresselhaus, A. Jorio, M. Hofmann, G. Dresselhaus, R. Saito, Perspectives on carbon nanotubes and graphene Raman spectroscopy, Nano Lett. 10 (2010) 751–758, https://doi.org/10.1021/nl904286r.

[34] K. Derelizade, F. Venturi, R.G. Wellman, A. Khlobystov, T. Hussain, Structural changes of thermal sprayed graphene nano platelets film into amorphous carbon under sliding wear, Appl. Surf. Sci. 528 (2020), 146315, https://doi.org/10.1016/j.apsusc.2020.146315.

[35] A. Mulone, I. Ennen, A. Hütten, U. Klement, In-situ TEM annealing of amorphous Fe-24at.%W coatings and the effect of crystallization on hardness, J. Mater. Sci. (2020), https://doi.org/10.1007/s10853-020-05485-7.

[36] C. Lee, X. Wei, J.W. Kysar, J. Hone, Measurement of the Elastic Properties and Intrisic Strength of Monolayer Graphene, Science (80-.). 321 (2008) 385–388.

[37] M.A. Krishnan, K.S. Aneja, A. Shaikh, S. Bohm, K. Sarkar, H.L.M. Bohm, V.S. Raja, Graphene-based anticorrosive coatings for copper, RSC Adv. 8 (2018) 499–507, https://doi.org/10.1039/C7RA10167H.

[38] Y. Zhao, Y. Tang, M. Zhao, L. Liu, C. Gao, C. Shuai, R. Zeng, A. Atrens, Y. Lin, Graphene Oxide Reinforced Iron Matrix Composite With Enhanced Biodegradation Rate Prepared by Selective Laser Melting, 1900314 (2019) 1–5. 10.1002/adem.201900314.